Available online at www.sciencedirect.com
ScienceDirect
Food Chemistry 106 (2008) 1366–1374
Food Chemistry
www.elsevier.com/locate/foodchem

Real-time mapping of moisture migration in cereal based food systems with A_w contrast by means of MRI

W.P. Węglarz [a,*,1], M. Hemelaar [a], K. van der Linden [a], N. Franciosi [a], G. van Dalen [a], C. Windt [b], H. Blonk [a], J. van Duynhoven [a], H. Van As [b]

[a] *Unilever Food and Health Research Institute, Unilever R&D, Olivier van Noortlaan 120, P.O. Box 114, 3130 AC Vlaardingen, The Netherlands*
[b] *Laboratory of Biophysics, Wageningen University, Wageningen, The Netherlands*

Received 12 October 2006; received in revised form 13 April 2007; accepted 16 April 2007

Abstract

The redistribution of water in prototype food systems, comprising phases with contrasting water activity (A_w), was investigated. To accomplish this task, MRI techniques adapted to migration rate were used. RARE and SPI measuring methods were used to monitor water redistribution in crunchy inclusions in water and biscuit shells with apple filling during storage, respectively. In the first case, fast migration, which typically last some tens of minutes, was monitored with a temporal resolution 3.5 min or better, while in the second case of slow migration it was monitored during 2 months with 10 days temporal resolution. 3D MR images with sub-millimeter resolution visualise the spatial redistribution of moisture and allow a quantification of its rate and extent of matrix swelling. Correlation with high resolution X-ray (XRT) images allows to identify structural elements responsible for unwanted fast hydration.

The obtained results demonstrate the potential of a combined MRI/XRT approach for dynamical monitoring of the migration of moisture into porous cereal material in a broad range of A_w contrast and hydration levels. The measured migration rates through samples of different internal structures can be used for validating models for prediction of water redistribution in multiple phase systems in a quantitative manner.

Keywords: Cereal material; Water activity contrast; Water (re)distribution; MRI; RARE; SPI; XRT

1. Introduction

Moisture migration between components with different water activity is a very important issue for preserving food quality during storage and/or preparation (Labuza & Hyman, 1998; Roos, Leslie, & Lillford, 1999). The *thermodynamic* description of this problem, based on the concept of differences in water activity (A_w), is well established (Guillard, Broyart, Guilbert, & Gontard, 2003). On the other hand, the *kinetics* of moisture migration is less well understood. Currently, the role of meso- and micro-structure on migration kinetics is recognised. No general predictive models have been developed however, primarily due to the absence of measurement techniques that can measure moisture distribution in real-time, non-invasive and quantitative manner. Magnetic resonance imaging (MRI) is ideally suited for non-invasive imaging of water, and has found broad range of applications in different areas, recently also in food science (Cornillon & Salim, 2000; Eads, 1998; Hills, 1998; Horigane et al., 2006; Ruan & Chen, 1998; Troutman, Mastikhin, Balcom, Eads, & Ziegler, 2001). An appropriate choice of the MRI measuring method and its parameterisation are required to allow visualisation of slow as well as fast migration processes and to recognise different transport mechanisms (Mohorič et al., 2004; Ramos-Cabrer, van Duynhoven, Timmer, & Nicolay, 2006; Ziegler, MacMillan, & Balcom, 2003). When relaxation is taken into account in an appropriate manner,

* Corresponding author. Fax: +48 12 6628458.
E-mail address: Wladyslaw.Weglarz@ifj.edu.pl (W.P. Węglarz).
[1] On leave from the Institute of Nuclear Physics, Kraków, Poland.

0308-8146/$ - see front matter © 2007 Elsevier Ltd. All rights reserved.
doi:10.1016/j.foodchem.2007.04.077

this allows for mapping of the spatial distribution of the molecular mobility of water (Ruan et al., 1996; Watson, Hollenshead, & Chang, 2001).

The aim of this work was to monitor redistribution of water in prototype food systems, comprising phases with contrasting water activity (A_w), by using MRI techniques adapted to migration rate and hydration level. Two extreme cases were chosen: big A_w contrast with subsequent fast hydration and lower A_w contrast with slow hydration. These were realized using crunchy inclusions in a hot water environment and biscuit shells with a moist apple filling, respectively. To accomplish the task, fast spin echo (RARE) and single point imaging (SPI) measuring methods were used to monitor water redistribution. In addition, X-ray tomography (XRT) was used for assessment of the fine structure of the non-hydrated samples in order to correlate hydration properties with structural details (van Dalen, Blonk, van Aalst, & Luengo, 2003).

2. MRI methodology

2.1. Properties of NMR signal of hydrated cereal-based matrix

MR images are based on NMR signals sampled in the presence of magnetic field gradients in order to obtain spatial resolution. The NMR properties of the sample (i.e., proton density, T_2, T_1), as well as signal sampling algorithm (the MRI measurement method), define sensitivity and thus image contrast and temporal and spatial resolution (Blumich, 2000; Eads, 1998; Hills, 1998). Fig. 1 shows NMR time domain signals (T_2 decays) from a moderately hydrated cereal-based solid matrix. It is composed of a short – "solid" component disappearing after 50–100 μs depending on the sample, a long – "liquid" component with a T_2 above ~2 ms, and an intermediate component with a T_2 in the range roughly between 0.1 and 2 ms. The solid component originates from the protons in carbohydrate, protein and solid lipids constituting the matrix. The intermediate component in most cases describes water at low or moderate hydration level ($A_w < \sim 0.9$), while the liquid component corresponds to water that is not associated to the solid matrix and/or to liquid lipids usually present in cereal-based food materials (Fig. 1). For high hydration ($A_w > \sim 0.9$), the T_2 of liquid lipids, which is in order of few to hundreds ms, may be similar to that of water saturating the matrix (Hickey et al., 2006; Ruan & Chen, 1998).

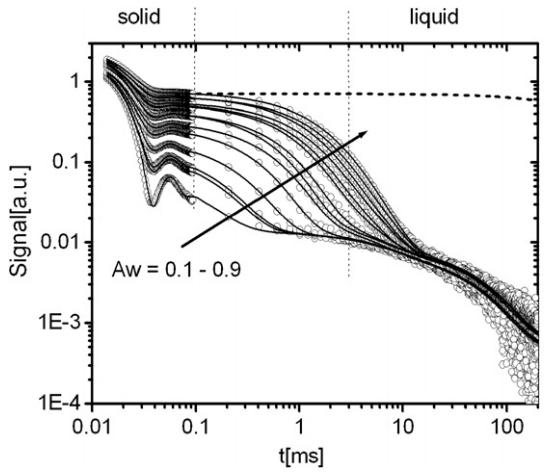

Fig. 1. Transversal NMR signal (T_2) decays from moderately hydrated cereal based matrix. The limit of water T_2 increase with further A_w increase is shown as dotted line corresponding to bulk water signal present in the sample.

2.2. MR imaging

In order to achieve spatial resolution, the time domain NMR signal needs to be sampled under influence of magnetic field gradients. The obtained 1D, 2D or 3D arrays of data points form time domain representations of the image of corresponding dimensionality, in the so-called "*k*-space". After complex Fourier transformation, the actual MR image is obtained. In order to fill *k*-space, an appropriate number of data points need to be collected. For "liquid" samples, with a long T_2, collecting all data necessary to build up the image is possible during a "one shot" experiment. In case of a signal with short T_2, which is typical for low – or moderately hydrated samples, many repetitions of the measurements are necessary in order to collect enough data (Blumich, 2000; Eads, 1998; Hills, 1998). Description of the MRI methodology used for investigations of food materials is available in the papers cited through out this text. Different methods can be used to optimally image samples exhibiting different ranges of water mobility (and thus hydration level). Here only a brief description is given of two methods, which are most adequate for addressing these measurement challenges, i.e. fast spin echo imaging and single point imaging.

2.2.1. Fast spin echo imaging method (FSE, TSE, RARE)

In fast spin echo imaging (also known as turbo spin echo or RARE) a CPMG train of echoes is used to obtain an image (Hennig, Nauerth, & Friedburg, 1986). For samples containing "liquid" components with a long T_2, this method can be very effective with respect to time- and space- resolution. A single image is produced from signals collected from multiple echoes, measured at different echo times. The possibility to adjust the number of echoes (RARE factor – RF) and the phase encoding scheme allows for enhancing or suppressing signals with different T_2. If the measured sample contains "liquid" regions with different T_2, like bulk water or a water-saturated porous matrix, this will result in a complicated dependence between obtained image contrast and experimental parameters. FSE is well suited for dynamic measurements of rapid (second-minute scale) hydration of cereal matrices (Mohorič et al., 2004). However, if signal from a water-saturated matrix (T_2 in order of tens of ms) needs to be enhanced in the image, then the temporal or/and spatial

resolution has to be compromised due to a limiting RARE factor. Suppressing of the signal from bulk water can be achieved by applying a short repetition time (TR) as compared to the T_1 of bulk water, which typically is in order of 1 s.

2.2.2. Single point imaging (SPI, SPRITE)

Unlike most of the spin-echo (or gradient echo) MRI methods, which are limited to measure the liquid signal only, SPI and its variant SPRITE use the FID signal (Balcom et al., 1996; Beyea et al., 1998; Deka et al., 2006; Emid & Creyghton, 1985; Troutman et al., 2001; Ziegler et al., 2003). SPI methods are based on frequently repeated measurements of a single point on the FID signal in the presence of gradients. A short encoding time ($t_e \ll 1$ ms) can be used, allowing for imaging of materials with intermediate T_2. This method can be used to image early stages of hydration, where the NMR signal from water has a T_2 in order of 1 ms or less. However, due to long experimental times, especially for 3D imaging at high resolution, it has limited application for dynamic (real-time) experiments in the second-minute scale.

Due to utilisation of small tilt angles (α) and usually fast repetition times (TR), the measured signal is highly dependent on both the intrinsic sample properties (e.g. T_2 and T_1) as well as the experimental setup (e.g. α, TR). In order to achieve adequate spatial resolution, short excitation pulse (t_p) and broad filter width (FW) are required (Gravina & Cory, 1994).

3. Materials and methods

3.1. Samples

3.1.1. Crunchy inclusions

Wheat flour based crunchy inclusions (0.5–1 cm in diameter, A_w of ~0.3) with different internal microstructures (denoted as type A, B, C) were produced locally, on pilot bakery scale. The differences in microstructure were achieved by application of different manufacturing processes to the same dough formulation. All samples were prepared in uncoated and coated forms. The coating consisted of a vegetable fat and acted as a moisture barrier. The A, B and C structures were coated with 11.7%, 10.9% and 16.3% w/w fat, respectively.

3.1.2. Biscuit shells with moist filling

Cereal based snack models with moist filling were produced locally on pilot bakery scale. The outer part of the sample is a biscuit shell, moulded in two parts (a cup and a lid), that could be sealed together. A flour/fat/sugar ratio of 100/34/15 was used to make a dough that was suitable for lamination. The shells (A_w of ~0.3) were coated internally with a layer of lipid material (Grindsted® Barrier System 2000, Danisco, Denmark), which is a blend of wax and acetylated monoglyceride, and filled with a moist apple based compote (Carrels, $A_w = 0.98$, 9% sucrose).

3.2. XRT – structure assessment

The internal porous structures of the crunchy inclusions used for hydration experiments were visualised using a SkyScan 1072 desktop X-ray micro-tomography (XRT) system (Belgium, http://www.skyscan.be). X-rays are generated by a microfocus X-ray tube (10 μm focal spot size) with tungsten anode operating at voltage 50 kV and current 100 μA. The transmission of the conical X-ray beam through the sample is recorded by a CCD camera with 1024 × 1024 pixels. XRT produces two-dimensional images of projections of the sample. A set of flat cross sections were obtained after tomographical reconstruction of images acquired under different rotations over 180° with a step size of 0.45°. The acquisition time for one projection was 2.8 s resulting in a total acquisition and read-out time of about 40 min. Samples were imaged using plastic cylindrical sample holder with an inner diameter of 11.2 mm. For visualisation in 3-D space, volume and isosurface rendering were used (Amira 4.1 from Mercury Computer Systems).

3.3. MR imaging – hydration assessment

3.3.1. Crunchy inclusions

Assessment of hydration of the crunchy inclusions was accomplished using a 300 MHz Bruker DSX MRI system with a 3 cm rf resonator. A standard RARE sequence as supplied by Bruker was used, however acquisition parameters were tuned to enhance signal from water saturating the porous material of the sample.

Fig. 2 shows the scheme of the experimental setup used to follow hydration of crunchy inclusions once in contact with bulk water. Prior to each measurement, the individual, dry ($A_w = \sim 0.3$) crunchy inclusion was placed into a sample tube containing water with defined temperature and volume. After an initial check and eventually correction of NMR tuning, which takes up to 30 s, the sample was monitored for the time necessary to assess progress of hydration. To accomplish this, the temporal resolution of a RARE measurement method was tuned to the rapid rate of water redistribution at 25 and 60 °C. This was achieved by using short repetition (TR = 200 ms), and echo (TE = 1.8 ms) time and

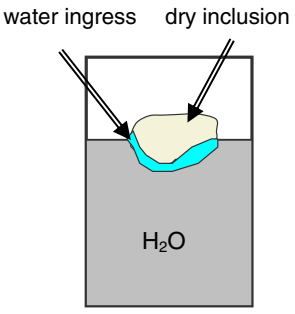

Fig. 2. Schematic depiction of the MRI experiment for assessment of crunchy inclusion hydration.

a RF of 4 and 8. A single scan measurement, i.e. no signal accumulation, was used, which allows for a temporal resolution of 3.5 min and 2 min, respectively. The use of a higher RF, which will allow for faster measurements, was not convenient as it suppresses signal from water saturating the porous matrix, while enhancing signal from bulk water surrounding it. A short repetition time was also beneficial for relative contrast enhancement of the water saturating the matrix. The higher temperature was used for fat coated samples in order to properly assess temperature effects such as fat melting. The obtained images with 3D spatial resolution of 0.3 mm allow the real-time visualisation of the spatial redistribution of moisture.

3.3.2. Biscuit shells with moist filling

The standard Bruker SPI method was used for investigation of water migration in biscuit shells with apple filling. To maximise the signal from the part of the sample with low water content (shell), a short encoding time of 100 μs was used. Together with a short repetition time (TR = 1 ms), flip angle ($\alpha = 1.6°$) and 64 repetitions it allows to obtain 3D image ($64 \times 64 \times 32$) with a spatial resolution equal to $\sim 0.6 \times 0.3 \times 0.8\ mm^3$ within 2 h 20 min.

4. Results and discussion

4.1. Crunchy inclusions hydration

3D XRT images with resolution of 15 μm were obtained, show clear differences in the internal structure of samples A, B and C (Fig. 3). Samples of type A contain a central void space surrounded with layers of relatively dense material. In types B and C, smaller voids (pores) were distributed more randomly through out the sample. Integrity of the fat coating was assessed by means of differences in X-ray attenuation between cereal matrix and fat coating. In most cases this revealed non-uniform coating of the product surface (Fig. 3).

The first set of MRI experiments were done on non-coated samples at 25 °C, in order to assess the effect of structure on hydration. Fig. 4 shows two extreme cases: fast, non-uniform hydration and slow, relatively homogenous hydration. Both samples were hydrated at the same conditions. In the first case, fast ingress of water occurs, which begins at a specific region of a sample, and was accompanied with swelling of the material. At some point this leads to "catastrophic failure" of the sample structure, and further fast hydration. In the second case, the integrity of the outer part of sample (crust) retards hydration significantly. Significant differences in hydration rate and behaviour could be attributed to differences in internal structure. Correlation of the dynamic MR images with XRT structural information, obtained from dry samples prior to hydration experiments, proves that regions of a thin crust, in proximity of big internal pores were in most cases responsible for unwanted fast hydration (see Fig. 3, left and Fig. 4, top).

Due to hydration and swelling, the volume of the bright regions of the MR images corresponding to water saturating the cereal matrix ($A_w > \sim 0.9$) is increasing, while the volume of non-saturated regions is decreasing. In most

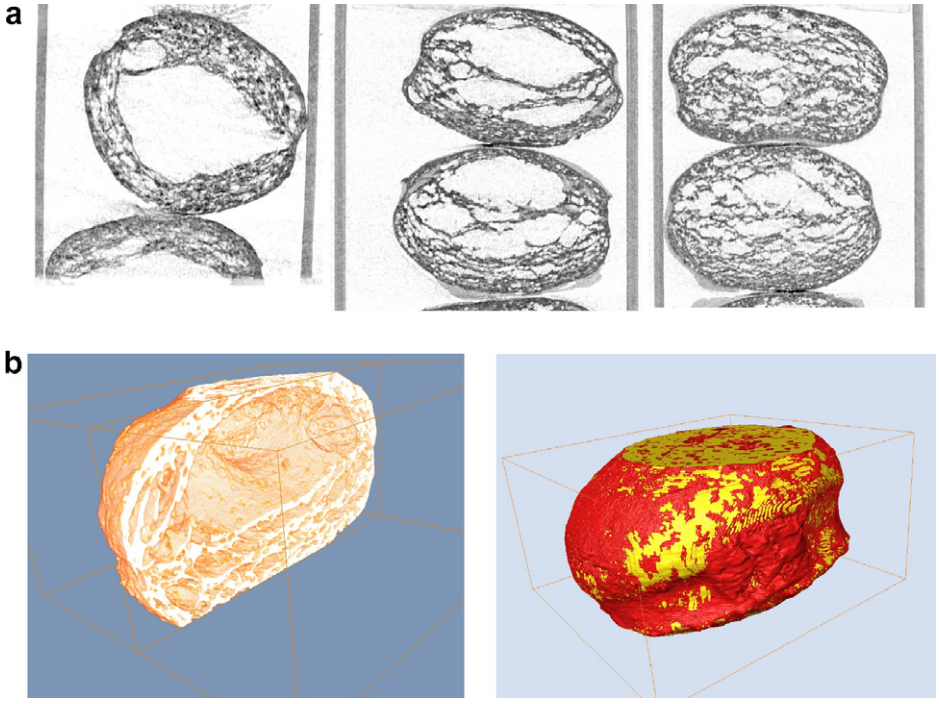

Fig. 3. (a) 2D vertical cross-sections through 3D XRT images of crunchy inclusions A, B and C (from left to right), (b) 3D XRT visualisation of internal structure (left) and non-uniform distribution of fat coating (red colour – right).

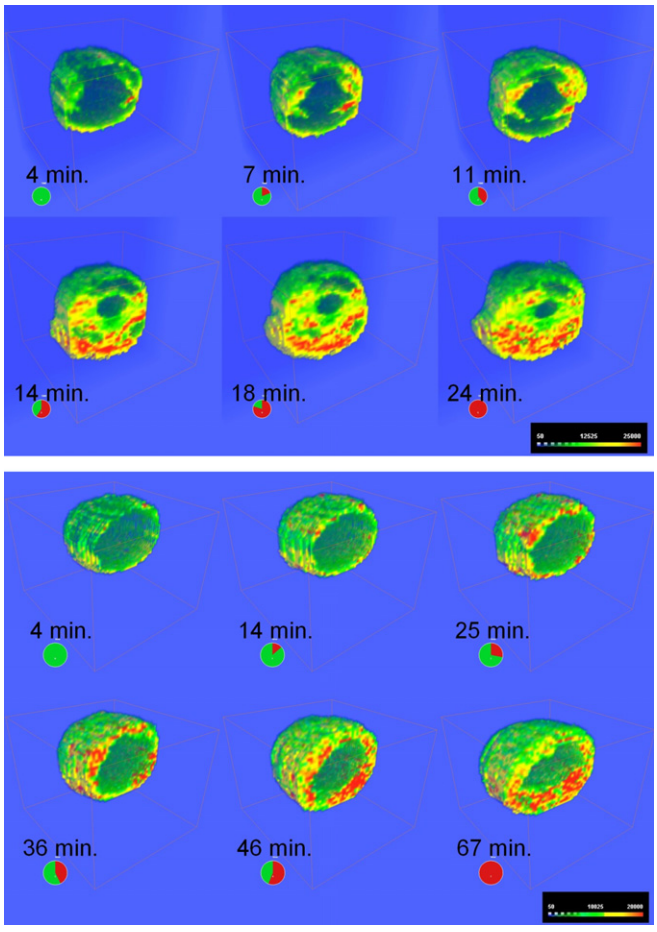

Fig. 4. 3D visualisation of MR images of crunchy inclusions hydration: (top) fast, "catastrophic" water ingress and (bottom) slow homogenous diffusion of water into inclusion structure. 3D structure clipped at centre of inclusion (box size = 13.5 × 10.8 × 13.5 mm). Color scale from green to red corresponds to A_w range between ~0.85 and 1.0.

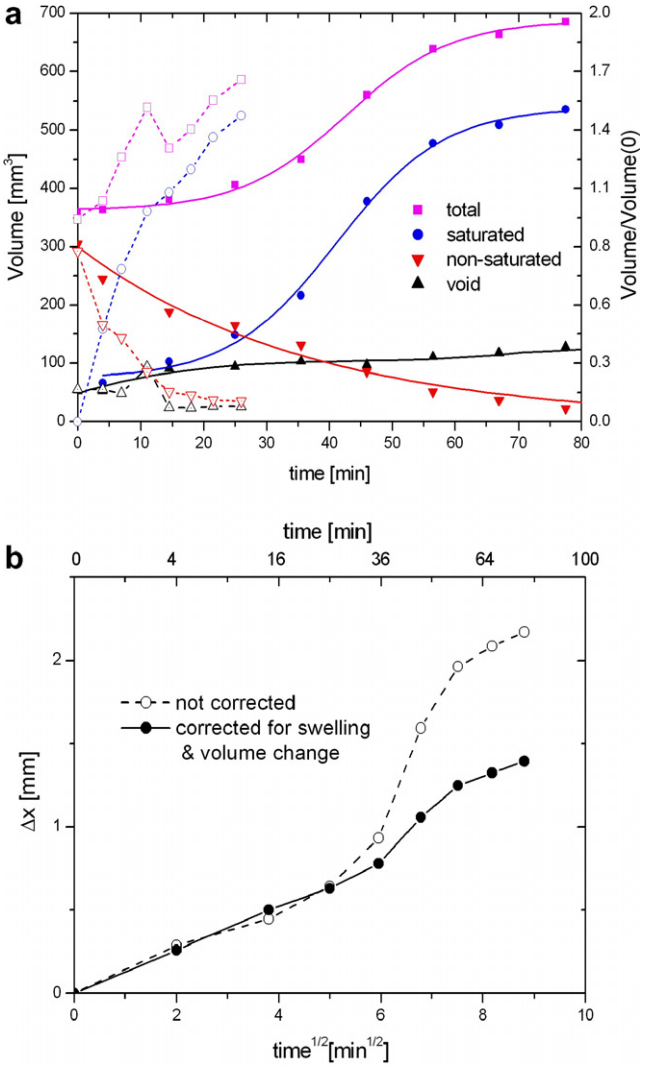

Fig. 5. (a) Kinetics of the uncoated crunchy inclusions hydration at 25 °C, show the volume change of different regions of the sample, for slow (continuous line, closed symbols) and "catastrophic" (dotted line, open symbols) water ingress. (b) Average displacement of hydration front for slow water ingress.

cases, the volume of the central void space filled with air also increased to some extent, unless air was released due to "catastrophic" hydration. In order to describe volumes changes, 3D MR images were segmented into different regions and the corresponding volumes were measured. Fig. 5a shows time dependence of volumes of the water-saturated region, the non-saturated region, the central void space, as well as the total volume of the sample. Two extreme cases of hydration shown in Fig. 4 are included in graph. The original (dry) volumes of the corresponding regions within both samples are very similar. Also the final volumes of the saturated and residual non-saturated regions are similar, however hydration kinetics are very different. In the case of slow hydration, the total and saturated volume change can be approximated by a sigmoidal curve, except for the very initial time during which faster increase of the saturated volume is observed. An approximately exponential decrease of the non-saturated volume is observed at the same time. From the fitted curves, characteristic times can be obtained to describe the hydration rate. A steady increase of the volume of central void space is also observed. In the case of the "catastrophically" failed sample, very fast increase/decrease of the volume of saturated/non-saturated regions is observed at the early stage of hydration. Breaking of the structure is accompanied with release of part of the air from central void, which is reflected in an abrupt decrease of the volume of void and total sample volume. The hydration rate of the matrix itself does not seem to be affected much by the structure breakdown, as can be concluded from the smooth increase of the volume of the saturated region. This suggest that it is the fast initial hydration which leads to the break-up of the structure due to tension between swollen and not yet hydrated material, rather than break of the structure facilitating fast hydration.

In order to assess the predominant mechanism for hydration, an average displacement of hydration front was calculated for the slow hydration case. Calculation

was based on rough assumption of the spherical shape of the sample as well as the hydration front moving from outside toward the sample centre. Analyses of the averaged displacement calculated from the volumetric data, rather than individual profiles, were chosen in order to minimise effects of local heterogeneities in hydration front. These are apparent not only for "catastrophic" hydration, but also for slow diffusion case (Fig. 4). The calculated displacement was corrected for the effect of material swelling, as well as for increasing of the volume of the central void. The corresponding values are shown in Fig 5b. The initial dependence of the average displacement on the square root of time is linear at the beginning stage. Such behaviour is considered to be typical for capillary driven hydration in porous media, as predicted by the Washburn model (Lago & Araujo, 2001). Occurrence of swelling complicates the application of this approach in our sample. However, comparison with the data which were corrected for volume increase shows that effect of swelling is significant at the later stage of hydration. It is accompanied with an additional acceleration of hydration, the effect which is opposite to the situation in the non-swelling porous material.

The second set of measurements were done on coated samples, at 60 °C, in order to assess the effect of the fat coating on retarding hydration. Also in this case some fast, "catastrophic" hydrations were observed, however in general these were less frequent than for non-coated samples. Fig. 7 shows a set of MR images of coated inclusions during a hydration experiment. Due to the NMR properties of melted fat (short T_1 as compared to water) its signal is enhanced over the bound and bulk water signal, and appears on MR image as the brightest region. The images show predominantly slow homogenous ingress of melted fat into the crunchy inclusions, preventing hydration. However, it also shows a region on the surface from which faster hydration begins, leading to premature hydration of the entire sample. Correlation with XRT images proves that regions of the sample surface which were poorly coated were responsible for faster initial hydration (see Fig. 6).

The above examples show that for the investigated material, the hydration behaviour of the individual samples of the same type may differ significantly. In order to assess the effect of differences in structure, the presence of coating and temperature on hydration behaviour, a larger set of inclusions was used for further experimentation. Samples of all three types (structures A, B and C, respectively), differing in pores (void) sizes and distribution were divided into three groups, which were measured at different conditions. Hydration of non-coated samples was assessed at

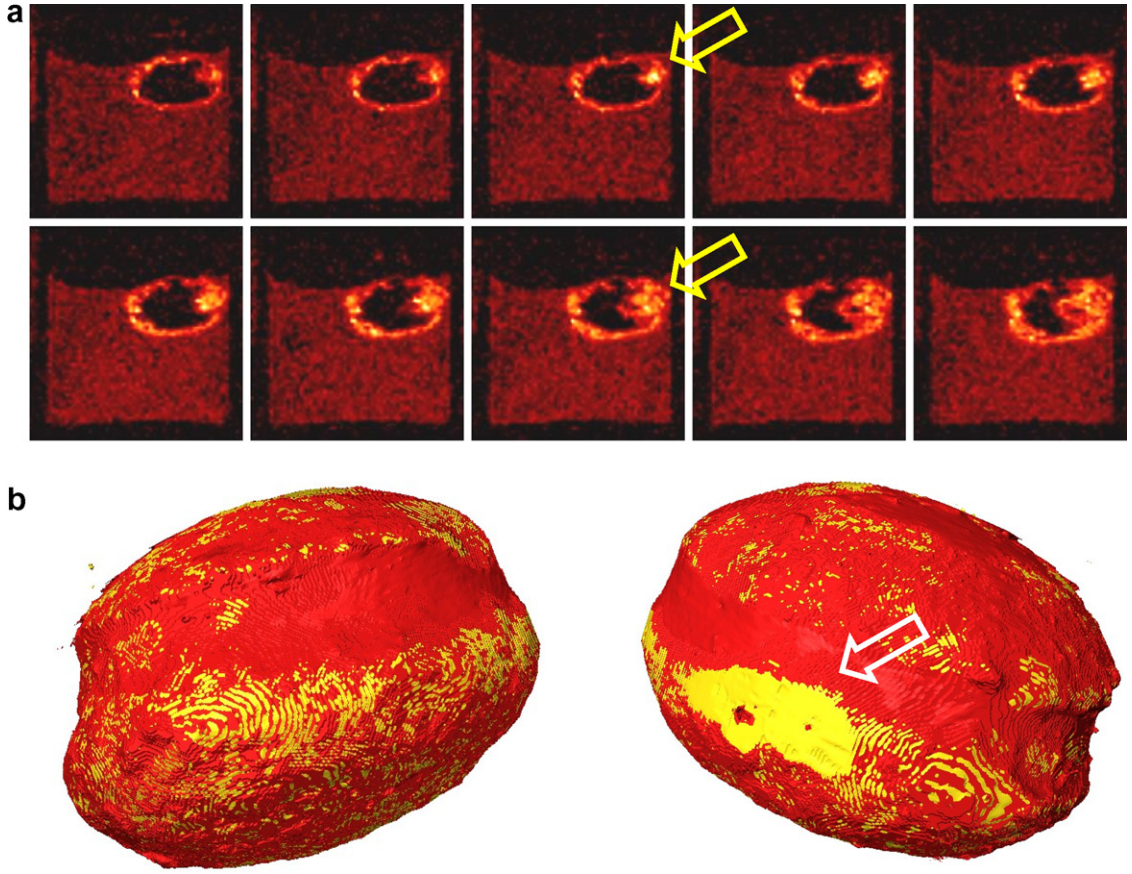

Fig. 6. (a) Correlation of the dynamic MR images of crunchy inclusions hydration with (b) XRT images show an uncoated region of the sample surface (in yellow on XRT images).

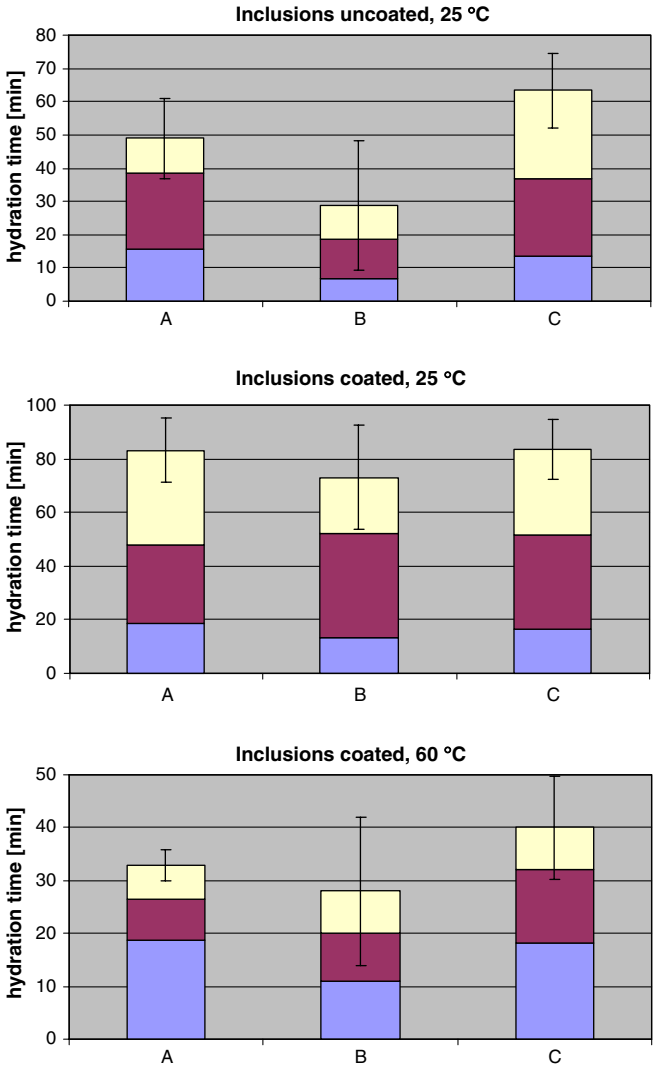

Fig. 7. Dependence of the hydration time of a crunchy inclusions on internal structure (A, B, C), presence of fat coating and temperature. Hydration progress were characterised by the time during which saturation volume reached 10%, 50% and 90% (initial, middle and final hydration stage, respectively) of the total inclusion volume (excluding big central void).

25 °C, while coated ones were investigated at 25 and 60 °C. In each group 4–6 inclusions with specific (i.e., A, B, C) structures were used. Hydration rates were characterised by the time during which saturation volume reached 10%, 50% and 90% (initial, middle and final hydration stage, respectively) of the total inclusions volume (excluding big central void). Fig. 7 shows comparison of hydration time for three groups of samples. Samples with the same structure (i.e., A, B or C) and hydrated at the same conditions display significant differences in hydration. This is reflected in relatively high standard deviation of the average hydration time. However, in every group, inclusions based on a B structure exhibit the worst performance (shortest hydration time). This is especially visible for non-coated inclusions at 25 °C. Application of a fat coating retards the hydration rate approximately 1.5–2 times, and decreases differences in average hydration rate between inclusions of different structure. The hydration rate of coated inclusions at 60 °C is roughly two times faster than at 25 °C. Also characteristic differences in relative hydration times for different stages of hydration are visible. At 25 °C, the fat coating apparently limits availability of bulk water for hydration during middle and final hydration stages, which is reflected in their relatively long duration. On the opposite, at 60 °C, once the bulk water finds a way to access the interior of sample through the melted fat area, hydration is relatively fast.

The presented results show that RARE method is well suited for assessment of the rapid hydration of the cereal material at high moisture conditions. Due to the complicated dependence of the signal on relaxation parameters (i.e., T_1, T_2) full distributions of relaxation time T_2 cannot be obtained in straightforward way. It allows however for dynamic visualisation of the hydration progress and allows for its quantitative description.

Correlation of the dynamic MR images of hydration progress with high resolution XRT images of dry samples allows recognition of structural details that determine hydration behaviour.

4.2. Water migration in biscuit shells with moist filling

In the case of hydration of crunchy inclusions, fast 3D MR imaging with adequate spatial resolution allows only for visualisation of water-saturated regions of the sample, which are hydrated predominantly through capillary and bulk water. In the case of cereal shells with moist filling and a fat barrier between them, these mechanisms are not important (or even not present at all in most cases). Much slower vapour phase hydration of the cereal matrix plays crucial role. As there is no bulk water in direct contact with the cereal matrix, the range of the A_w values is also lower (typically between 0.3 and 0.7). In such conditions, the short T_2 of the water (typically below 1 ms) excludes spin-echo based MRI method from being used effectively. The SPI method, based on FID signal should be used instead (Eads, 1998; Ramos-Cabrer et al., 2006; Troutman et al., 2001; Ziegler et al., 2003).

The effect of moisture migration in biscuit shells with apple filling and a barrier was monitored for ~3 months. Fig. 8 shows four consecutive SPI images of such a sample, obtained 11, 29, 50 and 86 days after assembling. The signal with the highest intensity in the central part of the sample corresponds to moist apple filling (original $A_w \sim 0.98$). Another region of relatively high intensity, especially visible in the lid shell (left side of the images) is attributed to the liquid fat which was used to saturate the inner part of the shell in order to retard water migration from the filling. The outer part of the shell without additional fat enrichment has significantly lower intensity. Also the barrier which is present between filling and inner part of the shell has lower intensity as it consists of solid fat mostly. During the time course, changes of the signal intensity in

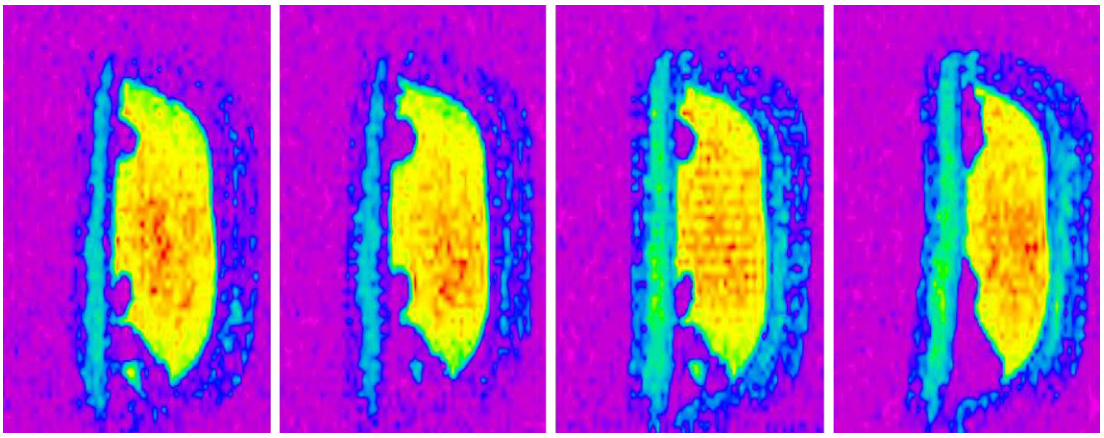

Fig. 8. Time series of SPI images of the biscuit shells with apple filling and a barrier obtained 11, 29, 50 and 86 days after assembling.

barrier and shell appear. Significant increase is visible especially between 29 and 50 days. This MRI observation was correlated with softening of the shell material in sample lid, which was detected before the last measurement. The corresponding A_w of the shell at the end of time series increased to 0.64 from the original 0.35 at the time of sample assembling, while the A_w of apple filling decreased from 0.98 to 0.92.

Fig. 9 shows the relative signal increase in the outer and inner part of the shell as well as in the barrier, calculated from the SPI data. The most significant increase of the signal amplitude is observed in the barrier being in direct contact with moist filling and in the inner, fat enriched part of the shell. The outer part of the shell seems to be less affected. This may be due to fact that the moisture is transferred through this region relatively easily to the surrounding air, which results in drying out of the outer part of the shell. Similar behaviour during starch moulding was reported in (Ziegler et al., 2002). The obtained results show the usefulness of the SPI method for assessment of the water migration in multi-component food systems with A_w contrast.

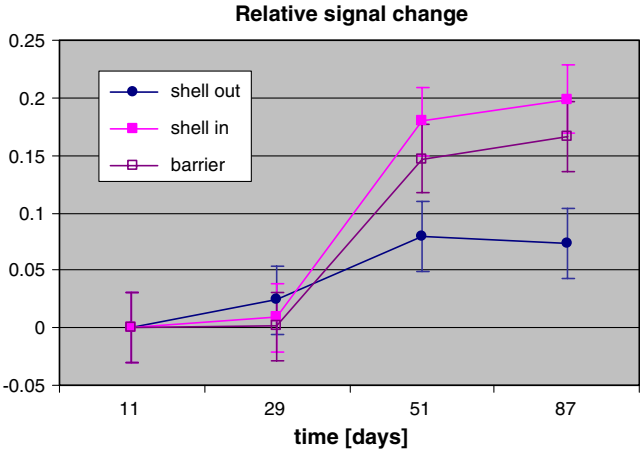

Fig. 9. Relative signal change during three months of storage, in different regions of a biscuit snack with apple filling.

5. Conclusions

The obtained results demonstrate the potential of MRI for monitoring and quantitative description of the migration of moisture in multi-component food systems with A_w contrast. MRI allows for dynamic visualisation of water ingress, but methods need to be chosen carefully and tailored for hydration level and desired temporal resolution.

Combination of dynamic MR images of hydration progress with high resolution X-ray images of crunchy inclusions allows identification of critical microstructural features that are responsible for unwanted fast hydration. In most cases the regions of thin crust are responsible for unwanted fast hydration. Such regions of thin crust serve as a path for fast water hydration of the interior part of the inclusion. This leads to accelerated swelling of the inclusion internal material and in some cases to fast, "catastrophic" hydration. Capillary action was found to be the predominant mechanism of hydration at an early stage. At a later stage it is followed by swelling of the material, which opens additional pathways for water to diffuse into the structure.

Gradient of the hydration which was changing with time was observed through out the biscuit shell. The outer part of the shell, exposed to air showed a limited increase in hydration. A significantly higher increase of hydration level was detected in the inner part of the shell, near the lipid barrier separating shell from moist filling.

In the presence of liquid lipids in the product, care should be exerted in interpretation of the image contrast in terms of water presence.

Acknowledgements

Supported by European Community within the framework of a Marie Curie Intra-European Fellowship (MEIF-CT-2005-009475). Dr. Peter Weegels (Unilever) is acknowledged for critical reading of the manuscript.

References

Balcom, B. J., MacGregor, R. P., Beyea, S. D., Green, D. P., Armstrong, R. L., & Bremner, T. W. (1996). Single-point imaging with T1 enhancement (SPRITE). *Journal of Magnetic Resonance Series A, 131*, 131–134.

Beyea, S. D., Balcom, B. J., Prado, P. J., Cross, A. R., Kennedy, C. B., Armstrong, R. L., et al. (1998). Relaxation time mapping of short $T2^*$ nuclei with single-point imaging (SPI) methods. *Journal of Magnetic Resonance Series A, 135*, 156–164.

Blumich, B. (2000). *NMR imaging of materials*. Oxford: Clarendon Press.

Cornillon, P., & Salim, L. C. (2000). Characterization of water mobility and distribution in low- and intermediate-moisture food systems. *Magnetic Resonance Imaging, 18*(3), 335–341.

van Dalen, G., Blonk, H., van Aalst, H., & Luengo, C. H. (2003). 3-D imaging of foods using X-ray microtomography. *G.I.T. Imaging and Microscopy, 3*, 18.

Deka, K., MacMillan, B., Ziegler, G. R., Marangoni, A. G., Newling, B., & Balcom, B. J. (2006). Spatial mapping of solid and liquid lipid in confectionery products using a ID centric SPRITE MRI technique. *Food Research International, 39*(3), 365–371.

Eads, T. M. (1998). Principles for nuclear magnetic resonance analysis of intact food materials. In M. Mossoba (Ed.), *Spectral methods in food analysis* (pp. 1–88). New York: Marcel Dekker.

Emid, S., & Creyghton, J. H. N. (1985). High-resolution NMR imaging in solids. *Physica B, 128*, 81–83.

Gravina, S., & Cory, D. G. (1994). Sensitivity and resolution of constant-time imaging. *Journal of Magnetic Resonance Series B, 104*, 53–61.

Guillard, N., Broyart, B., Guilbert, S., & Gontard, N. J. (2003). Evolution of moisture distribution during storage in a composite food, modelling and simulation. *Food Science, 68*, 958–966.

Hennig, J., Nauerth, A., & Friedburg, H. (1986). RARE imaging: A fast imaging method for clinical MR. *Magnetic Resonance in Medicine, 3*, 823–833.

Hickey, H., MacMillan, B., Newling, B., Ramesh, M., Van Eijck, P., & Balcom, B. (2006). Magnetic resonance relaxation measurements to determine oil and water content in fried foods. *Food Research International, 39*(5), 612–618.

Hills, B. (1998). *Magnetic resonance imaging in food science*. New York: Wiley.

Horigane, A. K., Naito, S., Kurimoto, M., Irie, K., Yamada, M., Motoi, H., et al. (2006). Moisture Distribution and Difusion in Cooked Spaghetti Studied by NMR Imaging and Diffusion Model. *Cereal Chemistry, 83*(3), 235–242.

Labuza, T. P., & Hyman, C. R. (1998). Moisture migration and control in multidomain foods. *Trends in Food Science & Technology, 9*, 47–55.

Lago, M., & Araujo, M. (2001). Capillary Rise in Porous Media. *Journal of Colloid Inerface Science, 234*, 35–43.

Mohorič, A., Vergeldt, F., Gerkema, E., de Jager, A., van Duynhoven, J., van Dalen, G., et al. (2004). Magnetic resonance imaging of rice during cooking. *Journal of Magnetic Resonance, 171*(1), 157–162.

Ramos-Cabrer, P., van Duynhoven, J. P. M., Timmer, H., & Nicolay, K. J. (2006). Assessment of water migration in multi-component snacks by magnetic resonance imaging. *Agricultural and Food Chemistry, 54*(3), 672–677.

Roos, Y. H., Leslie, R. B., & Lillford, P. J. (1999). *Water management in the design and distribution of quality food*. Lancaster, USA: Technomic Publishing.

Ruan, R., Almaer, S., Huang, V. T., Perkins, P., Chen, P., & Fulcher, R. G. (1996). Relationship between firming and water mobility in starch-based food systems during storage. *Cereal Chemistry, 73*(3), 328–332.

Ruan, R., & Chen, P. L. (1998). *Water in foods and biological materials. A nuclear and magnetic resonance approach*. Lancaster, USA: Technomic Publishing.

Troutman, M. Y., Mastikhin, I. V., Balcom, B. J., Eads, T. M., & Ziegler, G. R. (2001). Moisture migration in soft-panned confections during engrossing and aging as observed by magnetic resonance imaging. *Journal of Food Engineering, 48*(3), 257–267.

Watson, A. T., Hollenshead, J. T., & Chang, C. T. P. (2001). Developing nuclear magnetic resonance imaging for engineering applications. *Inverse Problems in Engineering, 9*(5), 487–505.

Ziegler, G. R., MacMillan, B., & Balcom, B. J. (2003). Moisture migration in starch molding operations as observed by magnetic resonance imaging. *Food Research International, 36*(4), 331–340.